This article has been accepted for publication in a future issue of this journal, but has not been fully edited. Content may change prior to final publication. Citation information: DOI 10.1109/LAWP.2020.3007527, IEEE Antennas and Wireless Propagation Letters

On Combining Attenuation Statistics of Different Tropospheric Effects Affecting EHF Earth-Space Links

Lorenzo Luini, Carlo Riva, Alberto Panzeri

Abstract— **Three attenuation statistics combination methods are evaluated and compared in this contribution for the first time using a consistent set of propagation data used as input and as a reference to test the methods' performance. The three approaches, which rely upon different statistical assumptions, aim at estimating the total tropospheric attenuation statistics by combining the complementary cumulative distribution functions of the attenuation associated to the different tropospheric impairments, namely clouds, gases, rain and scintillations. The prediction performance tests are conducted using as reference the propagation data (19.7 and 39.4 GHz) collected in Milan in the framework of the Alphasat Aldo Paraboni propagation experiment during 2017 and 2018. Results indicate that the combination method included in the inforce recommendation ITU-R P.618-13 provides the highest performance at both bands.**

Index Terms— **Radio propagation, total attenuation, atmospheric effects, troposphere**

I. Introduction

The evolution of Earth-space communication systems with operational frequencies beyond 10 GHz needs to cope with the significant impairments induced by the troposphere. Indeed, satellite and terrestrial telecommunication operators are increasingly interested in using higher frequency bands, such as the Ka and above, in order to meet the continuous growth in the larger bandwidth requested by the users; on the other hand, for such communication systems to be reliable, the impact of the different propagation impairments induced by the atmosphere needs to be adequately predicted [1]. Despite the predominant impact of the attenuation due to rain at any frequencies above 10 GHz, beyond 20 GHz also other tropospheric constituents, i.e. gases (namely water vapor and oxygen for frequencies up to 1 THz) and clouds, gain more and more importance, not only because they cause attenuation levels which can no longer be neglected in the system design process, but also due to their probability of occurrence, which is much higher than the one of rain [2].

Several prediction models have been developed so far to reliably estimate the statistics of the attenuation due to the individual constituents: for example, it is worth mentioning the methodologies for impairment prediction adopted by the International Telecommunication Union – Radiocommunication Sector (ITU-R) in recommendations P.676-12 for gases (A_G) [3], in P.840-8 for fog and clouds (A_C) [4] and in P.618-13 for rain (A_R) and scintillations (A_{SC}) [5]. The latter also includes a methodology aimed at combining the attenuation statistics due to the different constituents to obtain the total tropospheric attenuation, which is the key source of information for EHF (Extremely High Frequency) Earth-space link design. Such a methodology was devised by assuming some degree of correlation among the various components, but its accuracy was never properly tested on a consistent set of propagation data.

This works aims at addressing this point by evaluating the effectiveness of three attenuation statistics combination methods, which rely upon different statistical assumptions about the correlation among the various tropospheric effects. Specifically, the inforce recommendation ITU-R P.618-13 method [5], the procedure put forth in [6] and the proposed modification to recommendation ITU-R P.618-11 included in [7] are tested and compared using as reference the propagation data (19.7 and 39.4 GHz) collected in Milan in the framework of the Alphasat Aldo Paraboni propagation experiment during 2017 and 2018 [8],[9]. The key advancement offered by this work with respect to [6], which also focuses on assessing the accuracy of the attenuation combination methods, is the use of a consistent set of attenuation statistics associated to the different tropospheric constituents: the experimental total attenuation A is processed, on an instantaneous basis, to isolate its various contributions, hence to derive Complementary Cumulative Distribution Functions (CCDFs) of A_G, A_C, A_R and A_{SC}, which are afterwards recombined to obtain the CCDF of A according to the abovementioned models.

Following this introduction, Section II describes the experimental setup and how the experimental data were processed. Section III focuses on describing the different combination methodologies, whose prediction performance is compared in Section IV. Finally, Section V draws some conclusions.

II. Experimental Setup and Data Processing

A. Experimental Setup

This work relies on the propagation data collected during 2017 and 2018 in Milan, in particular on the power received (8 samples/second) at Ka band (19.7 GHz) and Q band (39.4 GHz)

Manuscript received XXXX.

Lorenzo Luini, Carlo Riva and Alberto Panzeri are with the Dipartimento di Elettronica, Informazione e Bioingegneria, Politecnico di Milano, Piazza Leonardo da Vinci 32, 20133, Milano, Italy (e-mail: lorenzo.luini@polimi.it).

This article has been accepted for publication in a future issue of this journal, but has not been fully edited. Content may change prior to final publication. Citation information: DOI 10.1109/LAWP.2020.3007527, IEEE Antennas and Wireless Propagation Letters

by means of the equipment installed by NASA Glenn Research Center at Politecnico di Milano (latitude 45.48° N, longitude 9.23° E, altitude 137 m a.m.s.l.) in the framework of the Alphasat Aldo Paraboni propagation experiment [9]. The beacon receivers are equipped with 1.2-m (Ka band) and a 0.6-m (Q band) Cassegrain antennas, and implement open-loop tracking to follow the Alphasat satellite, which is geosynchronous with orbital position at 25° E, but flying along an inclined equatorial orbit. In addition, a 4-channel (23.84, 31.4, 72.5 and 82.5 GHz) microwave radiometer (MWR) is collocated with the beacon receivers and is also pointed at the Alphasat satellite, with an average elevation angle of 35.6° [10]. Besides collecting brightness temperature data at the four frequencies (1 sample/second), under rainy-free conditions, the MWR also allows estimating the integrated liquid water content and the integrated water vapor content along the path. The same instrument also features meteorological sensors to monitor the pressure, temperature and relative humidity at ground level.

B. Extraction of the Single Attenuation Contributions

The total tropospheric attenuation at EHF is due to gases, clouds and hydrometeors (mainly rain); moreover, also scintillations contribute to a reduction in the received power for approximately 50% of the time [11]. In this work, the single contributions of the total tropospheric attenuation are isolated from the time series at both bands by means of the approach detailed in [12], to which the reader is addressed for more details. Here it will suffice to recall the main elements of such a methodology.

First, using a well-established approach, the total tropospheric attenuation A is estimated from the beacon received power P_R with the support of the MWR data, which are used to estimate the reference tropospheric attenuation A^{MWR} in rain-free conditions [10]. The scintillations A_{SC} are isolated by high-pass filtering A with a typical cut-off frequency of 0.03 Hz [11]. The remaining attenuation, containing the contributions of gases (A_G), clouds (A_C) and rain (A_R), is processed to first isolate $A_{RC} = A_C + A_R$ as follows:

$$A_{RC} = A - A_{SC} - A_G^{MWR} \tag{1}$$

where A_G^{MWR} is the gaseous attenuation estimated from the radiometer, in turn obtained as:

$$A_G^{MWR} = A^{MWR} - A_C^{MWR} = A^{MWR} - a_L L \tag{2}$$

In (2), A_C^{MWR} is the MWR-estimated cloud attenuation, which is obtained by using the liquid water mass absorption coefficient $a_L(f)$ (0.391 dB/mm at 19.7 GHz and 1.338 dB/mm at 39.4 GHz, as extracted from recommendation ITU-R P.840-8 [4]) and the liquid water content integrated along the path L, which is estimated using the well-established linear inversion procedure reported in [13]. Both L and A^{MWR} are valid only in rain-free conditions, thus the value of A_G^{MWR} in (2) is first interpolated between the beginning and the end of each rain event [14].

Afterwards, the attenuation due to clouds and the one due to rain are calculated as [12]:

$$A_C = \begin{cases} R_{RC} A_{RC} & A_{RC} \le A_{RC}^{max} \\ A_C^{max} & A_{RC} > A_{RC}^{max} \end{cases} \tag{3}$$

$$A_R = A_{RC} - A_C \tag{4}$$

where:

$$R_{RC} = a\ exp(-bA_{RC}) + (1-a)\,exp(-cA_{RC}) \tag{5}$$

Fig. 1 shows the trend of R_{RC} for both frequencies, while Table I lists the coefficients a, b, c, and the values of A_C^{max} and A_{RC}^{max} in (5) for both bands [12].

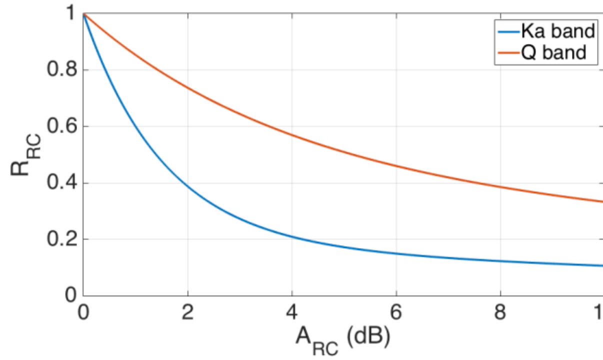

Fig. 1. Trend of R_{RC} as a function of A_{RC} for both frequencies [12].

TABLE I. COEFFICIENTS AND VALUES IN (5) [12].

	a	*b*	*c*	A_C^{max}	A_{RC}^{max}
Ka band	0.809	0.655	0.0596	1.1 dB	11 dB
Q band	0.569	0.259	0.0396	3.85 dB	16.9 dB

Finally, the attenuation due to water vapor A_V is given by:

$$A_V = A_G^{MWR} - A_{OX} \tag{6}$$

where the oxygen attenuation A_{OX} is estimated directly through the approximate yet accurate prediction model proposed in Annex 2 of the Recommendation ITU-R P.676-12 [3], which receives as input the ground pressure, temperature and relative humidity values collected by the weather station; the CCDF of the oxygen attenuation is then built from the instantaneous values of A_{OX}.

As an example, Fig. 2 depicts the CCDF of A_{OX}, A_V, A_C, A_{SC}, A_R and A at 19.7 GHz; all the CCDFs were calculated using the abovementioned procedure applied to the full propagation dataset described in Section II.A.

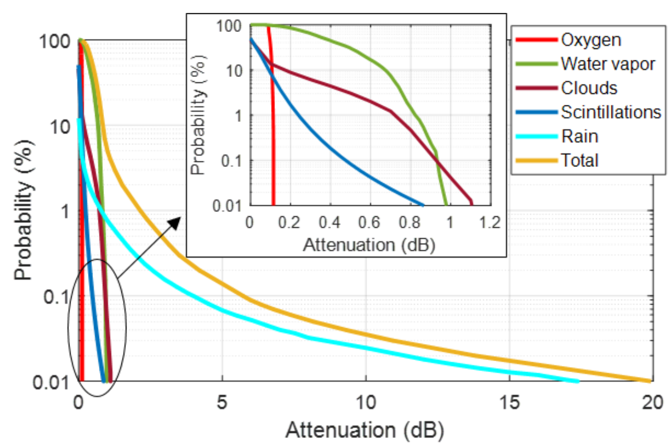

Fig. 2. CCDFs of the attenuation at 19.7 GHz: components and total.

Table II lists, for the Ka band (lower triangle of the matrix) and the Q band (upper triangle of the matrix), the correlation coefficient ρ for each pair of contributions of the total tropospheric attenuation: as expected, the results mainly point

This article has been accepted for publication in a future issue of this journal, but has not been fully edited. Content may change prior to final publication. Citation information: DOI 10.1109/LAWP.2020.3007527, IEEE Antennas and Wireless Propagation Letters

out quite a partial correlation between A_C and A_R (the latter is obviously not always concurrent with the former). On the contrary, scintillations appear to be poorly correlated with any other component, the highest ρ values being anyway associated to A_R and A_C. Finally, the attenuation due to gases is only slightly correlated to the other components, but results indicate quite a strong negative correlation between A_V and A_{OX}: this is due to their opposite dependence on temperature, and to the fact that both oxygen and water vapor are obviously always present in the troposphere.

TABLE II. CORRELATION COEFFICIENT AMONG THE DIFFERENT CONTRIBUTIONS OF TROPOSPHERIC ATTENUATION; KA BAND: LOWER TRIANGLE OF THE MATRIX; Q BAND: UPPER TRIANGLE OF THE MATRIX.

Ka/Q	Rain	Clouds	Water vapor	Oxygen	Scintillations
Rain	1	0.5990	0.0622	0.0036	0.0124
Clouds	0.4667	1	0.0339	0.1384	0.0070
Water vapor	0.0561	0.0324	1	-0.7673	-0.0006
Oxygen	-0.005	0.1427	-0.7694	1	0.0005
Scintillations	0.0090	0.0094	-0.0003	0.0003	1

III. ATTENUATION COMBINATION MODELS

Three different combination models are taken into account to predict the total attenuation statistics from the single contributions CCDFs discussed in Section II.B. The methodologies are different in terms of the statistical degree of correlation assumed among the different components but they all rely on the combination of the attenuation components at the same exceedance probability level.

A. Model 1

The reference model included in Section 2.5 of the inforce recommendation ITU-R P.618-13 assumes a quadratic summation of the contributions due to rain, clouds and scintillations, while the components due to water vapor and oxygen are assumed to be completely correlated. This is expressed by the following equation [5]:

$$A_1(P) = A_{OX}(P) + A_V(P) + \sqrt{[A_R(P) + A_C(P)]^2 + A_{SC}^2(P)} \quad (7)$$

It is worth pointing out that the methodology included in [5] also recommends to set $A_C(P) = A_C(1\%)$ and $A_G(P) = A_G(1\%)$ for $P < 1\%$: as stated in [5], this choice is intended to take into account that, for such a probability range, a part of the cloud attenuation and gaseous attenuation is already included in the rain attenuation prediction model proposed in the same recommendation. However, this is not the case considered in this work, where, on the contrary, $A_R(P)$ is assumed to be associated only to the rain attenuation component, according to what is discussed in Section II.B. Therefore, in this work, equation (7) is applied by considering the full range of values for all the attenuation CCDFs.

B. Model 2

The second combination method considered in this work assumes that the water vapor attenuation, the cloud attenuation and the scintillation effects are strongly correlated [6]. On the other hand, as shown in (8), the attenuation due to oxygen is always present and does not show significant variations; as a consequence, it is considered to be less correlated to the other effects and thus it is added separately:

$$A_2(P) = A_{OX}(P) + \sqrt{[A_V(P) + A_C(P) + A_{SC}(P)]^2 + A_R^2(P)} \quad (8)$$

C. Model 3

A modification to recommendation ITU-R P.618-11 was proposed in 2015 [7], in which the CCDFs of A_{RC} is assumed to be given by the sum of each exceedance probability P of A_R and A_C corresponding to the same attenuation thresholds A_i:

$$P(A_{RC} > A_i) = P(A_R > A_i) + P(A_C > A_i) \quad (9)$$

Equation (9) reflects the concept that the attenuation due to nonrainy clouds (A_C) cannot be present when rain is affecting the link (and viceversa); in fact, in [7], the contribution of rainy clouds to attenuation is assumed to be already included in A_R, which, in turn, is intended to be provided by a prediction model.

Such a contribution from clouds and rain is afterwards summed up quadratically to that of scintillations, while, as for Model 1, total correlation is assumed for the attenuation due to water vapor and oxygen. As a result, the combination of all the attenuation components is achieved as follows:

$$A_3(P) = A_{OX}(P) + A_V(P) + \sqrt{A_{RC}^2(P) + A_{SC}^2(P)} \quad (10)$$

IV. PERFORMANCE ASSESSMENT

Starting from the attenuation CCDFs associated to the single components derived in Section II.B, we have applied the three combination models described in Section III, to compare their output with the total attenuation statistics derived from the measurements collected in Milan at 19.7 GHz and 39.4 GHz (yellow curve in Fig. 2). Fig. 3 and Fig. 4 compare the measured and estimated statistics, at 19.7 and 39.4 GHz , respectively.

The models' prediction accuracy is quantified through the ITU-R P.311-14-defined error figure [15]- [17]:

$$\varepsilon(P) = \begin{cases} 100 \cdot \left(\frac{A(P)}{10}\right)^{0.2} ln\left(\frac{A_P(P)}{A(P)}\right) & A(P) < 10 \text{ dB} \\ 100 \cdot ln\left(\frac{A_P(P)}{A(P)}\right) & A(P) \geq 10 \text{ dB} \end{cases} \quad (11)$$

where, $A(P)$ and $A_P(P)$ represent the total attenuations, both correspondent to same probability level P, extracted from the measured and estimated statistics, respectively.

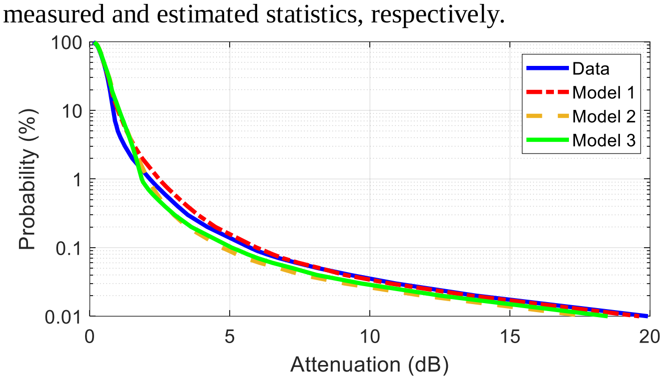

Fig. 3. Comparison between measured and predicted CCDFs of total attenuation at 19.7 GHz.

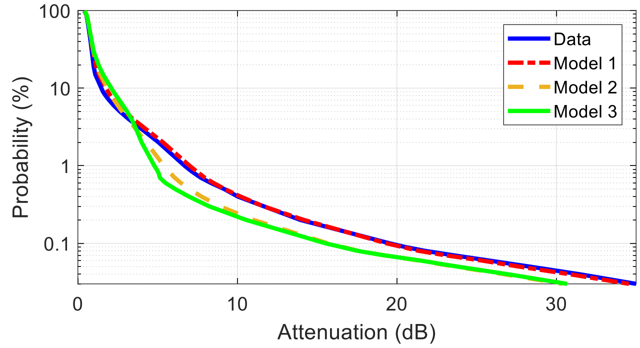

Fig. 4. Comparison between measured and predicted CCDFs of total attenuation at 39.4 GHz.

The higher accuracy of Model 1, clearly noticeable in Fig. 3 and Fig. 4, is confirmed by the results listed in Table III (left side of each cell), which includes, for both bands, the average (E) and root mean square (RMS) value of the error $\varepsilon(P)$, calculated on the probability range 0.01% $\leq P \leq$ 100% at 19.7 GHz, and 0.03% $\leq P \leq$ 100% at 39.4 GHz: the choice of a more limited P range at 39.4 GHz depends on the maximum dynamic range of the receiver, which is approximately 35 dB. Model 1 outperforms the other combination approaches at both bands, and its higher accuracy is even more marked at 39.4 GHz, where the RMS reduces from 22.5 (Model 3) to 5.6 (Model 1). The same trends are visible in Table III (right side of each cell), which also lists E and RMS for the customary relative error figure in (12), included for the sake of completeness:

$$\varepsilon_p(P) = 100\frac{A_P(P)-A(P)}{A(P)} \quad (12)$$

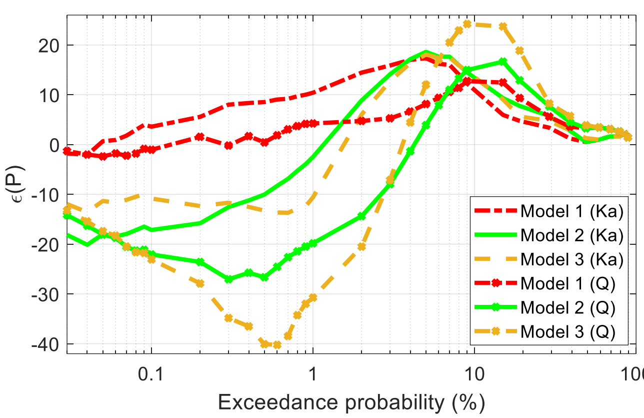

Fig. 5. Trend of the error figure $\varepsilon(P)$ as a function of the exceedance probability level at 19.7 GHz (lines with no markers) and 39.6 GHz (lines with markers).

Fig. 5 completes the models' performance assessment for both bands by depicting the trend of the error figure $\varepsilon(P)$ as a function of the exceedance probability level: the results point out a very good accuracy of Model 1 for $P <$ 0.1%, which is key for the reliable design of high-availability systems, while, in the same range of exceedance probability, Model 2 and Model 3 offer a much worse prediction accuracy. The maximum error delivered by Model 1, achieved in the 5% $\leq P \leq$ 10% range (definitely less critical for system design purposes), is approximately 17% and 11%, at 19.7 and 39.4 GHz, respectively.

TABLE III. AVERAGE (E) AND ROOT MEAN SQUARE (RMS) VALUES OF THE ERROR FOR THE THREE ATTENUATION COMBINATION MODELS; IN EACH CELL: ERROR FIGURE IN (11) ON THE LEFT, ERROR FIGURE IN (12) ON THE RIGHT

	19.7 GHz		39.4 GHz	
	E	**RMS**	**E**	**RMS**
Model 1	6.6/11.1	8.8/15.4	3.5/5.4	5.6/8.5
Model 2	-2.1/1.7	12.8/18.1	-7.9/-5.1	16.4/17.1
Model 3	-1.6/1.7	11.4/17.2	-9.1/-4.1	22.5/22.4

V. CONCLUSIONS

This contribution presented the evaluation of three attenuation statistics combination methods, whose performance is compared for the first time using a consistent set of propagation data used as input and as a reference for the tests. The three approaches rely upon different statistical assumptions to estimate the total tropospheric attenuation statistics by combining the complementary cumulative distribution functions of the attenuation associated to the different tropospheric impairments.

Two full years of data collected in Milan at 19.7 and 39.4 GHz in the framework of the Aldo Paraboni propagation experiment were processed to derive the total attenuation A. The various contributions due to gases, clouds, rain and scintillations were afterwards isolated, on an instantaneous basis, using a procedure taking advantage of the beacon receivers and the radiometer. The so-derived CCDFs of A_G, A_C, A_R and A_{SC} were afterwards recombined to obtain the CCDF of A according to the abovementioned models. The results clearly indicate that the combination method included in the inforce recommendation ITU-R P.618-13 provides the best performance at both bands, with an RMS of the error of 8.8 and 5.6 at 19.7 and 39.4 GHz, respectively, while the other models reach RMS values as high as 12.8 (Model 2 at 19.7 GHz) and 22.5 (Model 3 at 39.4 GHz). In addition, a more in-depth analysis of the outcomes shows a very good accuracy of Model 1 for $P <$ 0.1% (prediction error lower than 5%).

Though additional data (other sites, other frequencies) are needed to corroborate the results presented in this work, the performance of the inforce ITU-R P.618-13 combination method, which was never properly assessed so far, appears to be very satisfactory. Specific attention should be devoted to very low-elevation links (e.g. elevation angle $\theta <$ 10°), which characterize non-geosynchronous orbit systems and high-latitude ground stations for geosynchronous satellites. In fact, in principle, the degree of correlation among the various attenuation components underpinning (7) should be independent of the type of link considered. However, as the elevation angle decreases below 10°, the effects associated to scintillations increase significantly, and also multipath effects might play a relevant role: these aspects should be further investigated using additional beacon data collected at high-latitude sites along low-elevation links to confirm the accuracy of (7).

ACKNOWLEDGMENT

The authors would like to acknowledge: the Agenzia Spaziale Italiana (ASI), in particular Giuseppe Codispoti, for supporting the Alphasat Aldo Paraboni propagation experiment; NASA for making available the experimental data within the collaboration with Politecnico di Milano on the Alphasat Aldo Paraboni propagation experiment.

This effort was supported in part by the Air Force Office of Scientific Research, Air Force Material Command, USAF, under grant number FA9550-17-1-0335. The U.S Government is authorized to reproduce and distribute reprints for Governmental purpose notwithstanding any copyright notation thereon.

REFERENCES

[1] L. Luini, R. Nebuloni, and C. Riva, “Ka-to-W Band EM Wave Propagation: Tropospheric effects and Countermeasures,” in Wave Propagation Concepts for Near-Future Telecommunication Systems. InTech, 2017.

[2] C. Riva, C. Capsoni, L. Luini, M. Luccini, R. Nebuloni, A. Martellucci, “The Challenge of Using the W Band in Satellite Communication,” Int. J. Satell. Commun. Network. 2014; 32:187–200.

[3] ITU-R Recommendation P.676-12, “Attenuation by atmospheric gases,” ITU-R, Geneva, 2019.

[4] ITU-R Recommendation P.840-8, “Attenuation due to clouds and fog,” ITU-R, Geneva, 2019.

[5] ITU-R Recommendation P.618-13, “Propagation data and prediction methods required for the design of Earth-space telecommunication systems,” ITU-R, Geneva, 2017.

[6] L, Castanet, J. Lemorton, T. Konefal, A.K. Shukla, P.A. Watson, C.L. Wrench, “Comparison of various methods for combining propagation effects and predicting loss in low-availability systems in the 20–50 GHz frequency range,” International Journal of Satellite Communications. 19. 317 - 334. 10.1002/sat.703, 2001.

[7] United Kingdom of Great Britain and Northern Ireland, European Space Agency, “Proposed modification to recommendation ITU-R P.618-11,” Doc. 3J/130-E, 3M/227-E, Geneve, 15 April 2015.

[8] G. Codispoti, G. Parca, M. Ruggieri, T. Rossi, M. De Sanctis, C. Riva, L. Luini, “The role of the Italian Space Agency in investigating high frequencies for satellite communications: The Alphasat experiment,” International Journal of Satellite Communications and Networking, Special Issue: Alphasat Aldo Paraboni Ka and Q/V experiment, vol. 37, no. 5, Pages: 387-396, September/October 2019.

[9] M. Zemba, J. Nessel, C. Riva, L. Luini, G. Goussetis, “NASA's alphasat propagation terminals: Milan, Italy, and Edinburgh, Scotland,” International Journal of Satellite Communications and Networking, Special Issue: Alphasat Aldo Paraboni Ka and Q/V experiment, vol. 37, no. 5, pp. 502-512, September/October 2019.

[10] L. Luini, C. Riva, R. Nebuloni, M. Mauri, J. Nessel, A. Fanti, “Calibration and Use of Microwave Radiometers in Multiple-site EM Wave Propagation Experiments,” EuCAP 2018, 9-13 April 2018, pp. 1-5, London, UK.

[11] E. Matricciani, M. Mauri, C. Riva, “Scintillation and simultaneous rain attenuation at 12.5 GHz to satellite Olympus,” Radio Science, vol. 32, no. 5, pp. 1861-186, September-October 1997.

[12] L. Luini, A. Panzeri, C. Riva, “Enhancement of the Synthetic Storm Technique for the Prediction of Rain Attenuation Time Series at EHF,” accepted for publication in IEEE Transactions on Antennas and Propagation.

[13] L. Luini, C. Riva, C. Capsoni, A. Martellucci, “Attenuation in non rainy conditions at millimeter wavelengths: assessment of a procedure,” IEEE Transactions on Geoscience and Remote Sensing, pp. 2150-2157, Vol. 45, Issue 7, July 2007.

[14] X. Boulanger, B. Benammar, L. Castanet, “Propagation Experiment at Ka-Band in French Guiana: First Year of Measurements,” IEEE Antennas and Wireless Propagation Letters, Vol. 18, No. 2, pp. 241-244, 2019.

[15] ITU-R Study Group 3, “On testing variables used for the selection of prediction methods,” ITU-R, Fascicle Document 3M/FAS/1-E, July 2016.

[16] C. Capsoni, L. Luini, A. Paraboni, C. Riva, A. Martellucci, “A new prediction model of rain attenuation that separately accounts for stratiform and convective rain,” *IEEE Transactions on Antennas and Propagation*, Vol 57, No. 1, January 2009, Page(s): 196 - 204.

[17] L. Luini, C. Riva, “Improving the Accuracy in Predicting Water Vapor Attenuation at Millimeter-wave for Earth-space Applications,” *IEEE Transactions on Antennas and Propagation*, vol. 64, no. 6, Page(s): 2487 - 2493, June 2016.